Characterisation of an inhomogeneously irradiated microstrip detector using a fine spot infrared laser

G. Casse, P.P. Allport, S. F. Biagi, T.J.V. Bowcock, A. Greenall, P.R. Turner*
Oliver Lodge Laboratory, University of Liverpool, P.O. Box 147, Liverpool L69 3BX, UK

Abstract

A prototype silicon microstrip detector with p-strip read-out on oxygen enriched n-type substrate has been partially irradiated using a 24 GeV/c proton beam at the CERN-PS accelerator. The detector has a semicircular shape with radial strip geometry. The peak fluence received by the detector was 4.6×10^{14} p/cm^2 though the non-uniform nature of the exposure left part of the detector unirradiated. The inhomogeneous irradiation introduced a damage profile in the detector approximating to that expected in the inner LHC region. High irradiation gradients are important to study as they can modify the electric field within the silicon. Of special interest are changes in the component of the electric field parallel to the strip plane but perpendicular to the strips, which lead to systematic shifts in the reconstructed cluster position. If these (flux and position dependent) shifts are sufficiently large they could contribute to a degraded spatial resolution of the detector. In order to quantify these effects a precise fine light spot infrared laser was used to investigate the charge collection properties of the sensor. Particular attention was devoted to the regions where a high gradient of the fluence introduced a large gradient in the effective local space charge. The results reported below place limits on the "distortions" due to non-uniform irradiation.

Corresponding author: Tel. +44(0)151 7943399, e-mail: gcasse@hep.liv.ac.uk

Characterisation of an inhomogeneously irradiated microstrip detector using a fine spot infrared laser

G. Casse, P.P. Allport, S. F. Biagi, T.J.V. Bowcock, A. Greenall, P.R. Turner
Oliver Lodge Laboratory, University of Liverpool, P.O. Box 147, Liverpool L69 3BX, UK

Abstract

A prototype silicon microstrip detector with p-strip read-out on oxygen enriched n-type substrate has been partially irradiated using a 24 GeV/c proton beam at the CERN-PS accelerator. The detector has a semicircular shape with radial strip geometry. The peak fluence received by the detector was 4.6×10^{14} p/cm^2 though the non-uniform nature of the exposure left part of the detector unirradiated. The inhomogeneous irradiation introduced a damage profile in the detector approximating to that expected in the inner LHC region. High irradiation gradients are important to study as they can modify the electric field within the silicon. Of special interest are changes in the component of the electric field parallel to the strip plane but perpendicular to the strips, which lead to systematic shifts in the reconstructed cluster position. If these (flux and position dependent) shifts are sufficiently large they could contribute to a degraded spatial resolution of the detector. In order to quantify these effects a precise fine light spot infrared laser was used to investigate the charge collection properties of the sensor. Particular attention was devoted to the regions where a high gradient of the fluence introduced a large gradient in the effective local space charge. The results reported below place limits on the "distortions" due to non-uniform irradiation.

I. Introduction

A semicircular detector with inner and outer radius of 8 and 42 mm respectively and with radial strips for measuring the azimuthal tracking (Phi) in a azimuthal and radial (R) cohordinate system has been prototyped. The detector was non-uniformly irradiated, with 24 GeV/c protons in the CERN-PS/T7 experimental area, to study the effects of an inhomogeneous damage profile, which introduces position dependent changes in the electrical properties of the device.

To study the position dependent properties (e.g. the depletion voltage and charge collection) in different areas of the irradiated sensor a precise method of injecting electron-hole pairs is necessary. An infrared laser system has been built that allows the sensor to be scanned using a fine light beam. The results of the study on a partially irradiated phi-type detector are presented below.

II. The prototype phi detector

The prototype phi measuring sensors are 300 μm thick, p-strip in n-bulk silicon, with a semicircular shape covering 182 degrees. The masks were designed at the University of Liverpool and the sensors were fabricated by Micron Semiconductor [1] using oxygen enriched (up to ~2×10^{17} cm^{-3}) [2] FZ silicon 6" wafer. The sensors are divided into inner and outer radial sections each containing 1024 strips (Fig. 1). The inner and outer p-implants strips are collinear and are AC coupled to a "first" metal layer. The outer strips have bond-pads at the outer radius of the sensor. The inner strips are routed to the bonding pads, also located at the outer radius of the sensor, via metal strips ("second" metal), insulated from the first metal by a >3μm thick dielectric layer. The routing lines from the inner section run in

between the strips in the outer section, so that the bonding pads have a pitch of 62 µm while the effective outer strip pitch is 124 µm. A few other details of the sensors are listed below:

- The pitch of the innermost end of an outer strip is ~55.5 µm.
- The pitch of the innermost and outermost ends of an inner strip are ~24.4 µm and ~55.5 µm respectively.
- The strip width increases with the radius. The width of the innermost end of an inner strip is ~12 µm and the outermost end is ~ 16.7 µm. The width of the innermost end of an outer strip is ~16.8 µm and the outermost end is ~ 37 µm.
- The detector is also divided in 8 sectors, each one with bonding pads for the 128 inner and 128 outer strips.

III. Inhomogeneous irradiation of the Phi detector

A schematic of the set-up used to irradiate the Phi detector with 24 GeV/c protons in the CERN-PS East Hall is shown in Fig. 2. A holder containing the detector was mounted in a motorised carrier (Shuttle) in the IRRAD-1 facility [3]. The Shuttle allows positioning of the detector in the beam with the beam centre aligned as shown in Fig. 2. The beam has a nearly Gaussian profile with a FWHM of approximately 2 cm. Fig. 3 shows the fluence profile as measured using the activated aluminium foil technique [4] during the irradiation. The error on the absolute magnitude of the fluence is about 10%. The sensor position relative to the beam centre is known to an accuracy of about 2mm.

It is well known that the radiation damage introduces changes in the detector reverse current and effective space charge (N_{eff}) (see for example [5,6]). The reverse current and, for high doses, N_{eff} increase proportionally to the fluence. As a consequence of the beam profile, the detector N_{eff} has a nearly Gaussian profile across the device.

IV. Experimental methods

a. The detector support

To study the various sectors of the detector using a single read-out chip with 128 channels, a dedicated rebondable support, an infrared laser system and a precise x-y table have been set-up. The support has been designed to allow the sensor to be rotated hence enabling each sector to be bonded in turn. A rebondable fan-in extension was added to permit multiple bonding to the chip fan-in.

A single chip with 128 channels was used to read-out the outer radial section. In order to study the effect of the routing lines (from the inner radial section) on the electrical properties of the detector, two sets of 10 read-out channels at both sides of each sector studied, were bonded to the outer strips and the intermediate routing lines alternatively. All the remaining channels were bonded to the outer strips only, leaving the routing lines floating.

b. Infrared laser set-up and mechanics

An infrared laser diode with 1060 nm wavelength was driven by an external pulse generator to deliver short (< 5 ns FWHM) pulses. The light was guided by a single mode optical fibre to a light splitter with three output lines delivering about 60%, 20% and 20% of the input intensity respectively. The 60% output was connected to a photodiode and monitored on the oscilloscope to check the stability of the laser power emission. A 6µm

diameter core fibre, terminated with an optical focuser of 12mm focal length, was coupled to one of the 20% output lines. The light beam had a slightly elliptical profile with full-width-half-maxima of 7 μm and 6.6 μm on the major and minor axes. The laser power output was adjusted to produce a signal corresponding to about 3 minimum ionising particles in the sensor.

The sensor was mounted on an x-y table perpendicular to the laser beam. Two micromanipulators allowed precise movement with a resolution of two microns.

c. The read-out system

The sensor was read-out by the SCT128 LHC speed electronics [7]. The output of the chip is a data stream of 128 channels divided into 25 ns time bins containing single channel information. This output was acquired by the LeCroy LC574AL 1GHz oscilloscope and averaged over 1000 sweeps to record the height of the signal. This technique strongly suppresses the effect of electronic noise.

The timing of the readout relative to the laser pulse was adjusted to optimise the signal size by mean of a time scan. A digital delay on the laser pulse was used to vary the time interval between the light injection and the trigger to the data acquisition. The signal was recorded for different trigger delay times allowing the shape of the signal to be deduced. This shape is compared to the design pulse shape in Fig. 4.

To study the noise level on the detector, the output of the chip with no injection of charge was recorded with a flash SIROCCO ADC clocked at 40MHz.

V. Experimental results

a. Full depletion voltage (V_{fd}) and effective space charge (N_{eff}) profile

The charge collection efficiency (CCE) allows the extraction of the local V_{fd} [8,9]. V_{fd} is proportional to N_{eff} according to

$$V_{fd}=q_0 w^2 N_{eff} / 2\varepsilon_{Si} \qquad (1)$$

where q_0 is the electron charge, w is the thickness of the detector and ε_{Si} is the dielectric constant of silicon.

The collected (cluster) charge was defined as the sum of the charge collected on a strip and the two neighbouring strips (and routing lines where they were connected) on each side. The CCE curves are normalised to the maximum charge collected at the maximum applied bias (500 V). This normalisation does not allow the evaluation of the charge deficit as a function of the fluence and it is here used only for presentation purposes. The evaluation of the V_{fd} is done by fitting the CCE curves as described in [8,9].

Fig. 5 shows an example of charge collection efficiency (CCE) curves with the fit to evaluate V_{fd} in three different positions and estimated radiation fluences ($<5\text{x}10^{13}$, $\sim1.2\text{x}10^{14}$, $\sim3.4\text{x}10^{14}$ p/cm^2) of the detector. The local value of N_{eff} was calculated according to Eq. 1. Fig. 6 shows the map of N_{eff} measured across the whole detector at the outer end of the outer radial section. The shape of N_{eff} closely follows the measured fluence profile. Between strip #570 and #670 the gradient of N_{eff} is positive (maximum gradient $\sim4.7\text{x}10^{12}$ cm^{-4}), while between strip #690 and #760 it is negative (maximum gradient $\sim-4.2\text{x}10^{12}$ cm^{-4}). Transverse component of the electric field generated by the inhomogeneity of the irradiation would thus be expected to be opposite direction in these two regions. The comparison of the CCE properties in these two regions enables the study of the effects of a transverse electric field,

which has opposite direction and than produces opposite shifts in the collected charge (as sketched in Fig. 6).

b. Noise

This measurement was not intended to determine the absolute level of the detector noise, but to study the possible settling of micro-discharges due to the strong difference in full depletion voltage in the non-irradiated (V_{fd} <50 V) and highly irradiated (V_{fd} >200 V) regions. The inhomogenously irradiated detector must be operated with a bias voltage that allows a sufficient charge collection in the most damaged part. After heavy irradiation a bias voltage exceeding 300 V can be required (see the charge collection curve for the most irradiated strip in Fig. 5). The application of a bias much larger than V_{fd} in the low fluence area implies the presence of high electric fields next to the read out strip. In this situation, noise due to micro-discharges [10] may be observed. The study of this effect is important because it could be the prime limitation in the bias voltage applied to the detector, reducing therefore the lifetime of the detector when employed in high and inhomogeneous radiation environment.

Fig. 7 shows the noise measured in outer radial sector 5 of the sensor (see Fig. 1) as a function of voltage. The noise is not flat across the chip because of the poor condition of the fan-in extension. Nevertheless it is possible to observe that in the high fluence region (strip >#580) the bias can be raised up to 350 V with no increase of the measured noise. In the lower irradiation (and V_{fd}) region the noise starts to increase for an applied bias of 200V.

c. Charge sharing between adjacent strips

A detailed study of the charge division between adjacent strips (called Left and Right for simplicity) has been carried out in different areas of the detector. The charge division has been evaluated using the pulse height as a function of the local coordinate x, defined as the distance in microns of the centre of the light spot from the centre of the left (L) strip. The following algorithm has been used to evaluate the ratio (η) of the charge seen by the right strip (R) to the total charge:

$$\eta = H_R \Big/ (H_R + H_L) \qquad (2)$$

where H_R and H_L are the height of the signals seen by the left and right strip respectively.

Figures from 8 to 13 show the η scan as measured in the outer end of the outer radial section. The intermediate Al routing line (17 μm wide) prevents the measurement in the mid way between the two strips.

Fig. 8 shows the η scan for a low-irradiated area (strips #244-245, fluence <<5x10^{13} p/cm^2). Fig. 9 refers to strips located in the inversion area where the gradient of N_{eff} is small (#490-491, fluence <5x10^{13} p/cm^2) and the depletion voltage is about 50 V. Fig. 10 is from an area where the gradient of V_{fd} is increasing from strip L towards strip R (#634-635, fluence 3.9×10^{14}p/cm^2). Fig. 11 is from strips located in the area where the gradient of N_{eff} is small but with a high radiation level (#690-691, fluence 4.4x10^{14}p/cm^2). Fig. 12 shows the area where the gradient is decreasing from strip L towards strip R (#760-761, fluence 2.2x10^{14}p/cm^2). Fig. 13 shows the comparison of the charge sharing scan in the non-irradiated area with the two highly irradiated areas with opposite N_{eff} gradient. The symmetry of the three curves respect to the centre of the η distribution is compared in order to evaluate a systematic shift in opposite direction of the data collected in the positive and negative gradient area. There is no evidence of an asymmetry and the maximum distortion in the reconstructed cluster position is less than 2μm (Fig. 13), which is compatible with the spatial resolution expected from this procedure.

The ISE [12] package was used to simulate the effect of the N_{eff} gradient on the charge collected in two adjacent strips (L and R) with a minimum ionising particle (mip) impinging in the mid distance between the strips and perpendicularly to the detector plane. The N_{eff} gradient was equal to the maximum found in Fig. 6 (4.8×10^{12} cm^{-4}). Fig. 14 shows the signal observed in strip L and R respectively with an applied bias of 300V. The difference in the signal height corresponds to a displacement of the impact point of ~1 μm from the mid point between the two strips, in agreement with the experimental data.

The strips #760-761 have been studied as a function of radial position in the outer radial section. Fig. 12, 15 and 16 show the η scan in the innermost, intermediate and outer part of the strip, where the pitch is 78 μm, 95 μm and 118 μm respectively. The irradiation was not collinear with the strips (Fig. 2) and there is a gradient along the strips as well as across them. Fig. 17 shows the CCE curves measured in the three positions, clearly indicating a difference in V_{fd}. This explains the difference in the behaviours of the η scan as a function of the applied bias for the different regions. In Fig. 15 and 16 the detector is non-depleted at 150 and 200 V (positions 1 and 2 of Fig. 17) and the points for these two bias voltages are well separated from the points measured at 400 V, when the detector is fully depleted. In Fig. 12 the detector is already depleted at 200 V (Pos. 3 of Fig. 17) and the set of data taken at 200 and 400 volts of applied bias almost superimpose each other.

In the η scan figures the solid line represents the curve for ideal resolution. It is apparent that the charge sharing between neighbour strips in the irradiated part of the detector is much closer to the ideal resolution when the detector is biased below depletion. The presence of a non-depleted layer next to the read out strips enhances charge division, as it is shown in Fig. 18, where the laser was focused between strips #740-741, close to the #741. A significant fraction of the charge is distributed over 4 strips at low bias voltages and decreases by increasing the bias. A similar situation is not found in non-irradiated detectors, where the charge division for bias voltages below and above full depletion is more similar (see η scan in Fig. 8).

The enhanced charge sharing in underdepleted irradiated detectors can be due to the presence of a high resistivity region between the read out strips and the depleted bulk (where a high electric field is present), which increases the AC coupling between the strips. After the type inversion of the detector bulk from n-type to p-type because of the radiation damage, in the highly irradiated regions the junction side migrates from the back plane of the detector towards the readout strips. When the detector is under-depleted a low electric field region separates the active volume from the read out strips (double junction effects [12] are of lesser importance and are not addressed here). This region corresponds to the non-active part of the detector and it is usually referred as non-depleted region. Nevertheless the concentration of free carriers is very low after irradiation making this region behaving as an insulator (as opposite to the non-depleted region of a non-irradiated detector which behaves as a conductor because of the high density of free carriers). An ISE simulation is shown in Fig. 19 to compare the electric field distribution and majority carrier concentration as a function of the applied bias voltage of an irradiated (4×10^{14} p cm^{-2}) silicon detector. The irradiation effects have been simulated by introducing electron and hole traps in the silicon band gap. The details of the simulation parameters (charge carrier cross section, trap density and energy level) are listed in Table 1. Three of the energy level parameters are taken from [13] and two of the midgap levels from global fits of the temperature dependent depletion voltage of data from [14]. The irradiated detector depletes at ~ 200 V and it can be observed that the majority carrier concentration in the non-depleted bulk never exceeds 10^8 cm^{-3}, while in the non-irradiated detector the free carrier density in the non-depleted bulk is equal to the doping level of the high resistivity silicon (~10^{12} cm^{-3}, Fig. 20).

d. Effect of the routing-line on the collected charge

The non-uniform irradiation permits the study of the effect of the routing lines on the charge collection as a function of the dose. The AC coupling characteristics of the irradiated detector can be influenced by the high resistivity properties of the non-depleted region, as described above. In particular, a small signal could be induced on the routing lines for ionising particles passing in the outer segment, due to the enhanced capacitive coupling of these metal lines through the dielectric bulk. The fraction of the signal measured on the routing lines as a function of the irradiation dose and of the bias applied to the detector has been studied.

When the detector has not inverted, the p-n junction, and therefore the high field region, is on the side of the implanted p-type strips. In the non-irradiated region of the detector no charge was observed on the routing line at any bias voltage. Some loss of the charge to the routing has been observed in the irradiated and type inverted region, as shown in Fig. 21. The highest charge observed on the routing line coincides with the highest fluence region. In general, the charge in the routing line decreases strongly with bias, and becomes negligible for bias voltages above V_{fd}. This supports the interpretation that the charge loss mechanism involves capacitive coupling through the low-field region. The effect disappears when the high electric field spans over all the detector volume (full depletion).

The ratio of the width of the routing line to the width of the read-out strips can influence the amount of the charge collected by the routing lines, because of a higher relative capacitance for high ratios. The width of the routing line is constant (17 μm) while the width of the outer strips increases with radius, as described in section II. Fig. 22 shows the ratio of the charge collected by the routing line to the total charge for five radial positions from the inner to the outer part of the detector. The strip width, as measured using the deficit of signal caused by the screening to the laser light from the metal read-out strip was 16, 20, 25, 30, 35 μm for position 1 to 5 respectively. The effect of the lower depletion voltage in the outer part of the strip is clearly shown by the earlier decrease of the signal on the routing line for the outer positions. The effect of the relative width of the routing line to the strip, which varies from ~1 to ~0.5 going outwards, is not evident (this would appear as a trend in the maximum charge observed on the routing line.)

VI. Conclusions

The infrared laser set-up is an effective tool for studying the effects of inhomogeneous irradiation on large area microstrip silicon detectors. The measurement of the charge collection properties across the irradiated detector allowed the reconstruction of the irradiation profile and the study of the local characteristic as a function of the gradient of N_{eff}.

The study of the charge sharing between neighbouring strips as a function of the local position gives a maximum limit of 2μm in the distortion of the resolution as a consequence of a transverse electric field resulting from inhomogeneous irradiation. This is in agreement with ISE simulation of the inhomogeneously irradiated detector.

Evidence has been found of increased charge sharing in the irradiated and type inverted part of the detector when biased below V_{fd}. The increased charge sharing is due to the high resistivity non-depleted bulk next to the read-out strip. The enhanced resolution implied by the increased charge sharing is not necessarily beneficial. Operating p-in-n sensors under-depleted after irradiation implies a large reduction in charge collection efficiency and it can lead to an insufficient signal to noise ratio, especially when high charge division is involved.

An alternate choice of the diode structure, like n-strips in n-bulk (n-in-n) or p-bulk (n-in-p), would greatly benefit the operation of irradiated detectors [15-17].

The measured shape of the noise at high bias voltages on the irradiated sector of the detector (where the V_{fd} varies from <50 V to >200V) is compatible with noise induced by micro-discharges. The micro-discharge effect depends on the strength of the electric field and not on the applied bias. With the same applied bias voltage the electric field is higher for lower V_{fd}. In this region the noise is inversely proportional to V_{fd} confirming the hypothesis on the origin of the noise.

The unique geometry of these detectors includes metal lines to route the innermost strips to the bonding pads located on the outer end of the detector. The metal lines run symmetrically between the outer strips. The effect of these metal lines on the charge collection has been studied. When the detector is type inverted and biased below depletion, a fraction of the total charge is seen by the routing line and therefore lost. This effect is suppressed when the detector is depleted. Moreover, this effect is not seen in the non-irradiated part, suggesting that it is correlated with the presence of the non-depleted layer next to the strips. In case of read-out from the junction side, as for n-in-n or n-in-p detectors, no charge loss in the routing lines is predicted, improving the performances for non-depleted operation, as compared with p-in-n detectors.

References

[1] Micron Semiconductors, 1 Royal Buildings, Marlborough Road, Lancing, Sussex, BN15 8UN (UK).
[2] G. Casse et al., Nucl. Instr. and Meth. A 438 (1999) 429-432.
[3] M. Glaser et al., Nucl. Instr. and Meth. A426 (1999)72-77. See also http://irradiation.web.cern.ch/irradiation/.
[4] E. Leòn-Floriàn et. Al. "Particle fluence measurements by activation technique for radiation damage", CERN-ECP/95-15.
[5] K. Gill et al. Nucl. Instr. and Meth. A322 (1992) 177-188.
[6] A. Chilingarov et al., Nucl. Instr. and Meth. A360 (1995) 438-444.
[7] J. Kaplon et al. IEEE Transact. On Nucl. Sci. 44 (1997)2 98.
[8] S. Martí I García et al., Nucl. Instr. and Meth. A473 (2001) 128-135.
[9] P.P. Allport et al., IEEE Trans. Nucl. Sci., vol. 48 (2001) 1007-1011.
[10] T. Oshugi et al., Nucl. Instr. and Meth. A342 (1994) 22.
[11] ISE Integrated System Emgineering, http://www.ise.ch/
[12] G. Casse et al., Nucl. Instr. and Meth. In Phys. Research A 426 (1999) 140.
[13] A. Hallén, N. Keskitalo, F. Masszi, V. Nágl, J. Appl. Phys. 79(8), 3906 (1996).
[14] K. Borer et al., CERN-EP/99-98
[15] S. Martí I García et al., Nucl. Instr. and Meth. A426 (1999)24-27.
[16] P. Allport et al., Nucl. Instr. and Meth. A435 (1999) 74-79.
[17] G. Casse et al., Nucl. Instr. and Meth. A487/3 (2002)225-230.

Table 1 Radiation induced defects used for the ISE simulation of irradiated silicon detectors. The trap density quoted here is for a fluence corresponding to $1x10^{15}$ 1MeV neutron equivalent cm^{-2}.

Trap type	Trap density [cm^{-3}]	Energy from mid band gap [V]	El. capture cross section [cm^{-2}]	Hole capture cross section [cm^{-2}]
Electron	$1.50\ 10^{15}$	0.39	$1.00\ 10^{-14}$	$5.50\ 10^{-13}$
Electron	$2.20\ 10^{15}$	0.13	$2.00\ 10^{-15}$	1.2010^{-14}
Electron	$3.60\ 10^{14}$	0.035	$1.20\ 10^{-15}$	$1.20\ 10^{-14}$
Hole	$3.24\ 10^{14}$	-0.045	$1.20\ 10^{-14}$	$1.20\ 10^{-15}$
Hole	$1.50\ 10^{15}$	-0.20	$1.50\ 10^{-14}$	$2.00\ 10^{-15}$

Figures

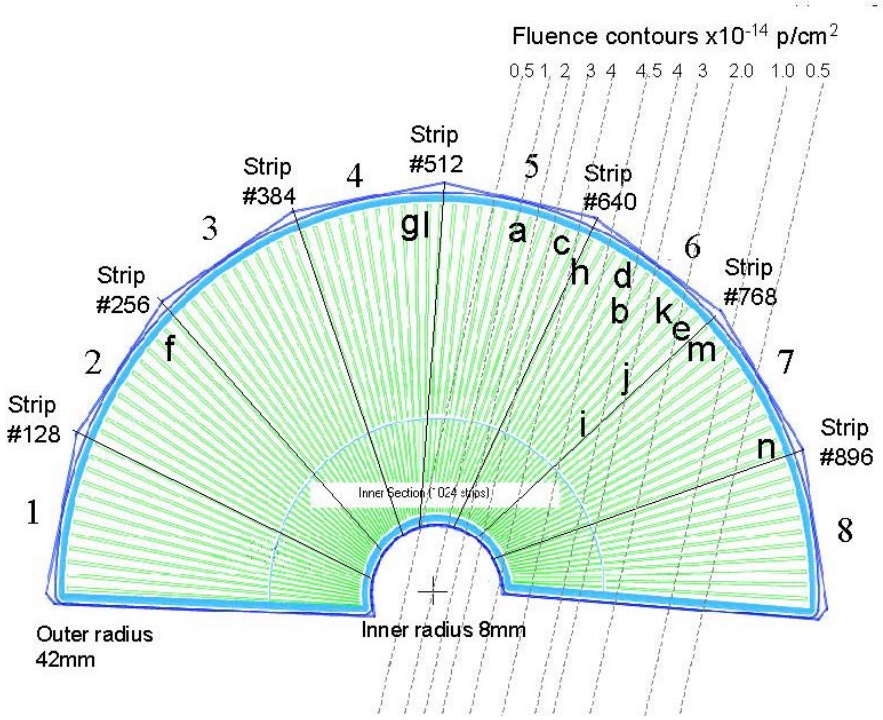

Fig. 1: *Schematic draft of the LHCb-Phi detector. Diagram contains approximate fluence contours for the irradiated detector and some indicative measuring positions labelled (a-n), most of which are along the outer radius of the sensor.*

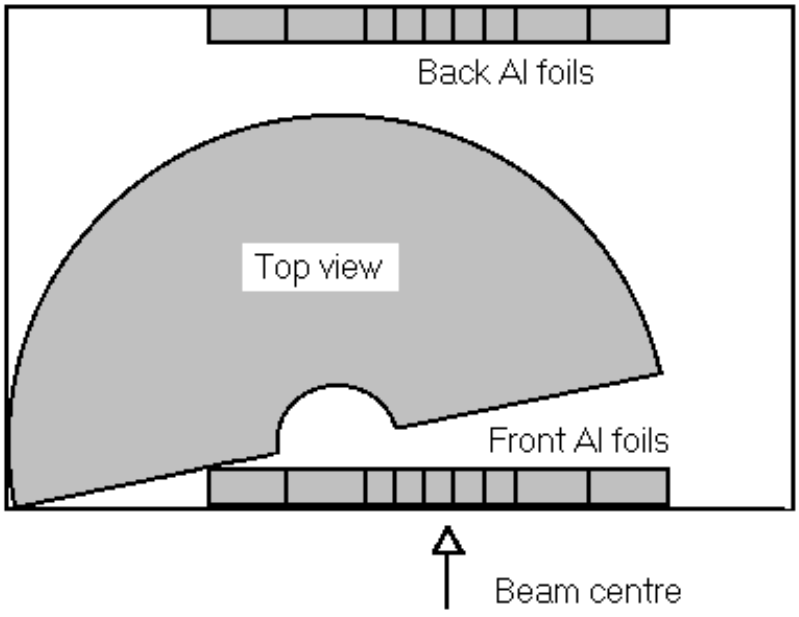

Fig. 2: *Diagram of the inhomogeneous irradiation set-up.*

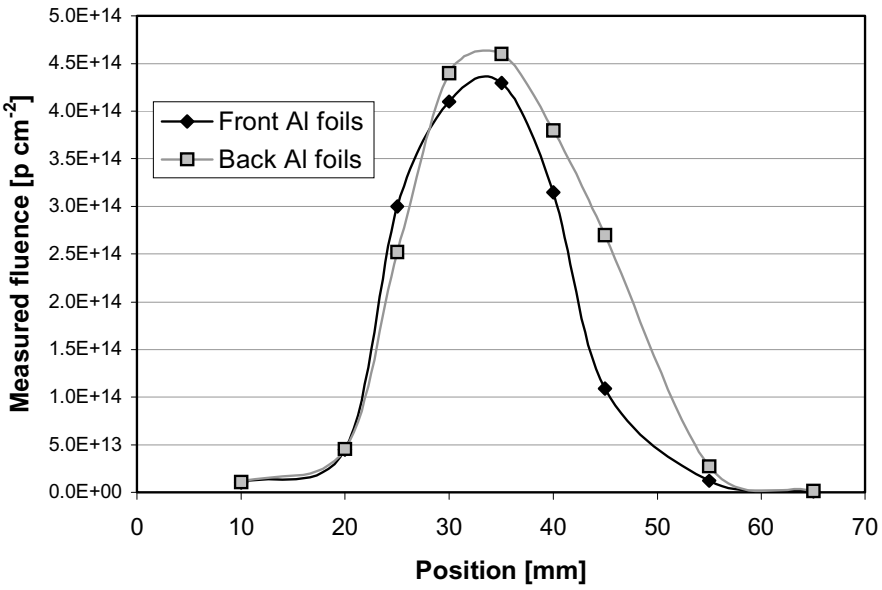

Fig. 3 *Beam profile as measured with the Al foils activation method on the before and after the beam crossing the detector.*

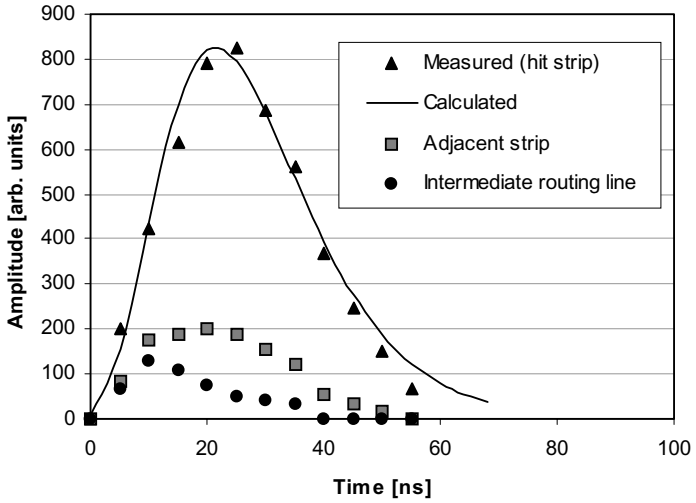

Fig. 4 *Time scan to reconstruct the pulse shape of the SCT128 chip. The solid line is the predicted SCT128a pulse shape. In the same plot are shown the hit strip, a neighbour one and the intermediate routing line.*

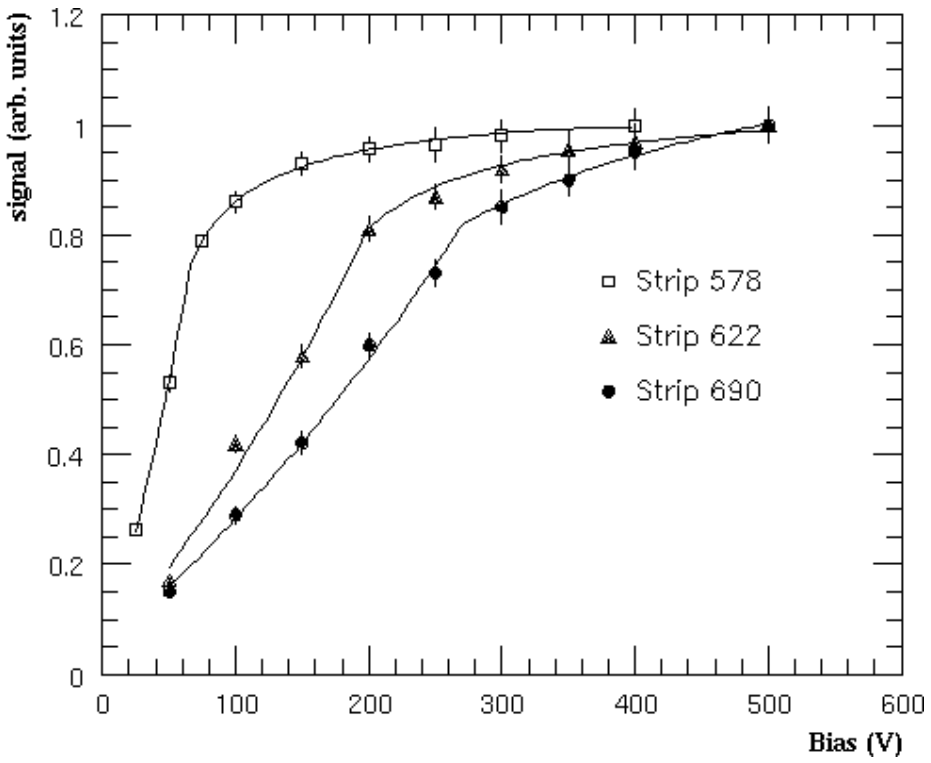

Fig. 5: *Sample of CCE curves in three different locations of the detector with different irradiation fluences. Strip #578 is in a intermediate fluence region, strip #622 in the region with maximum gradient of the fluence and strip #690 in the most irradiated region. The increase in the depletion voltage can be clearly seen. Strips #578, 622 and 690 were measured at positions* ***a, c*** *and* ***d*** *respectively (see Figure 1).*

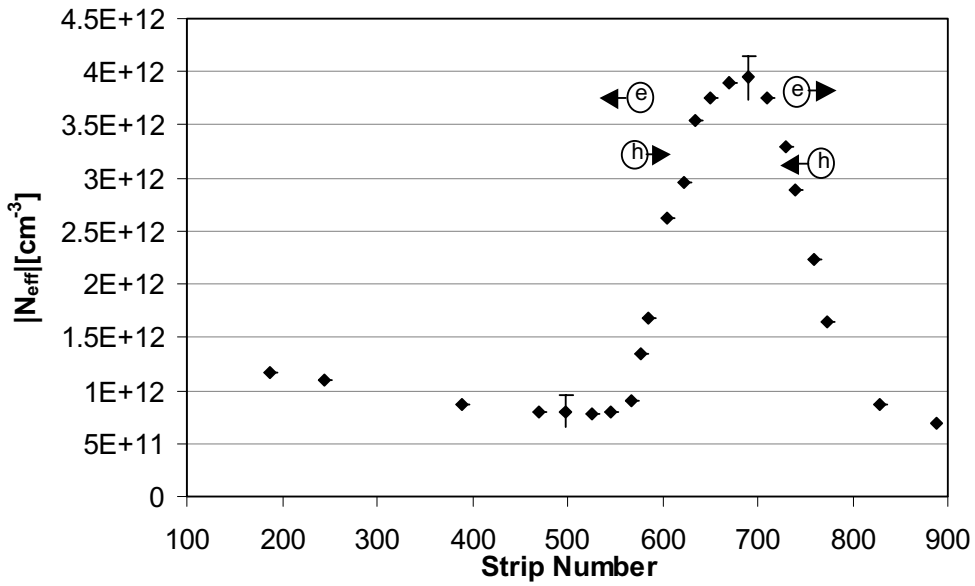

Fig. 6: *Absolute value of the effective space charge ($|N_{eff}|$) profile across the detector, as evaluated from the CCE curves measured on the outer end of the outer strips. Two typical error bars are shown for the low and high radiation damage regions. The profile matches the spatial irradiation profile. (Note Channels 580 to 800 span about 25mm).*
The p-type radiation induced defects introduce a negative space charge. The expected shift of the cluster charge due to the gradient of N_{eff} is sketched in the figure for electrons (e) and holes (h).

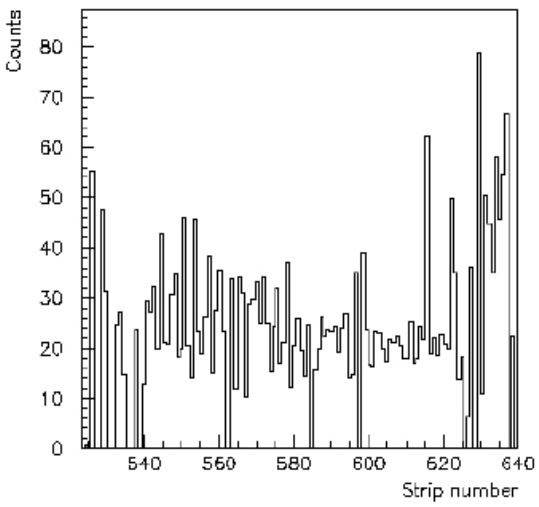

a) V=100Volts

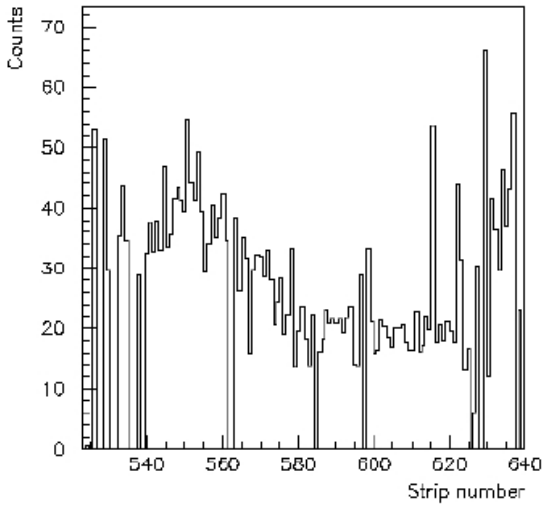

b) V=200Volts

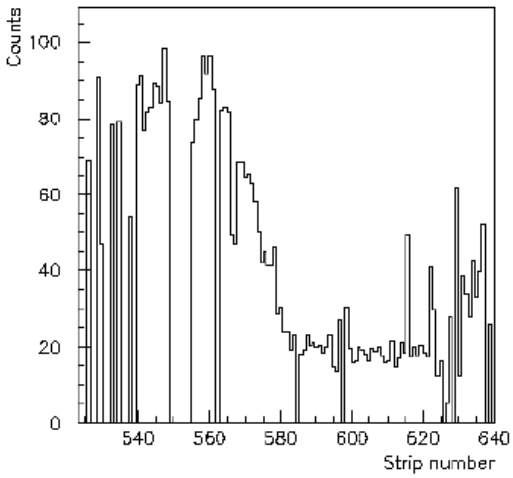

c) V=300Volts

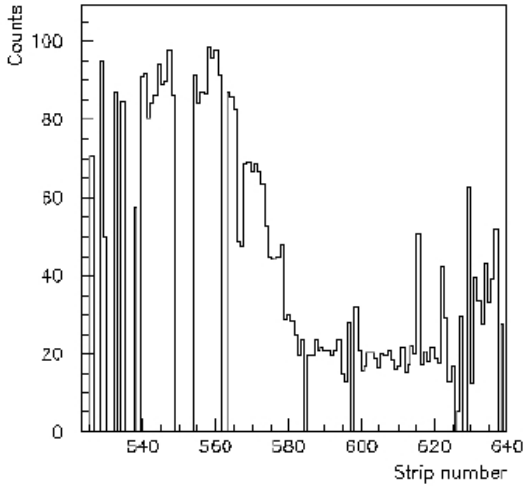

d) V=350Volts

Fig. 7: *Noise distribution in the sector number 5 of the irradiated detector at different bias voltages. In Fig. 12(c) and (d) the noise values for the strips between #549 and #559 (in the low fluence region) are missing because of an automatic masking, within the analysis program, of channels with extreme noise.*

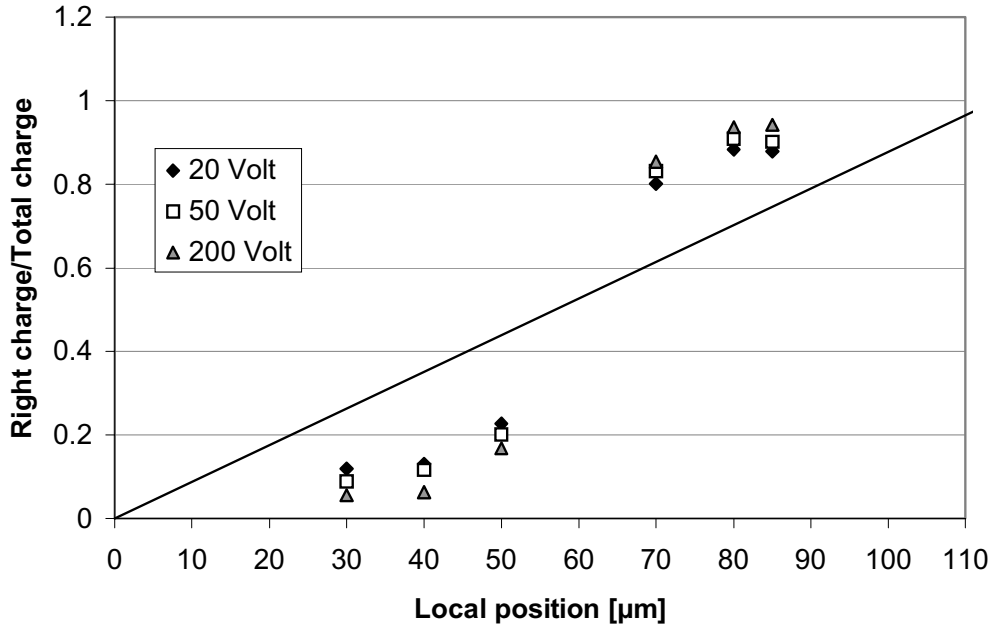

Fig. 8 *η scan across strip #244 – 245 (very low irradiation region) measured at position* ***f*** *(see Figure 1).*

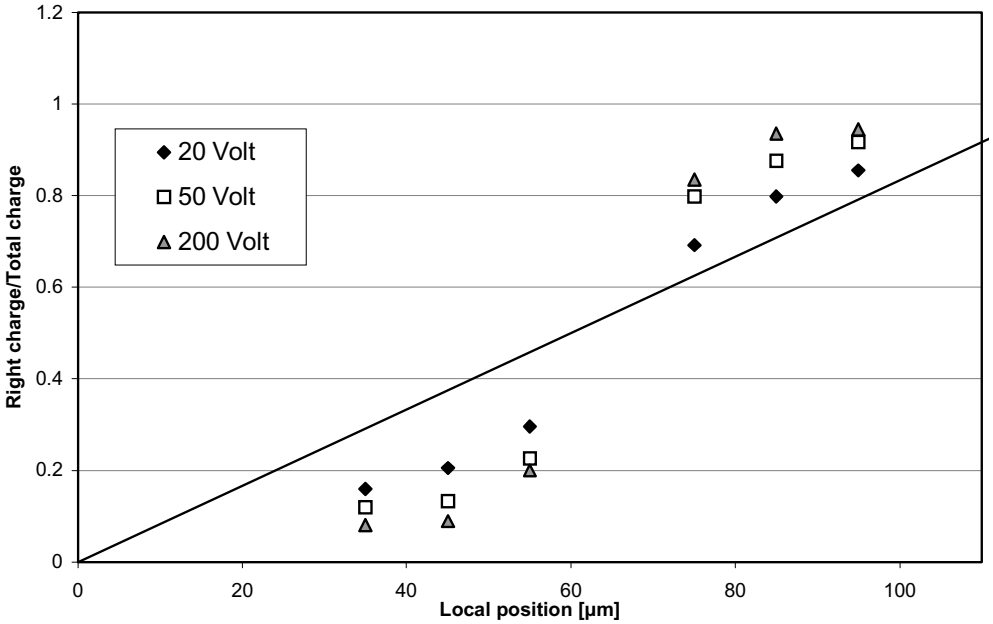

Fig. 9 *η scan across strip #490 – 491 (irradiated region with* V_{fd} *≈50V) measured at position* ***g*** *(see Figure 1).*

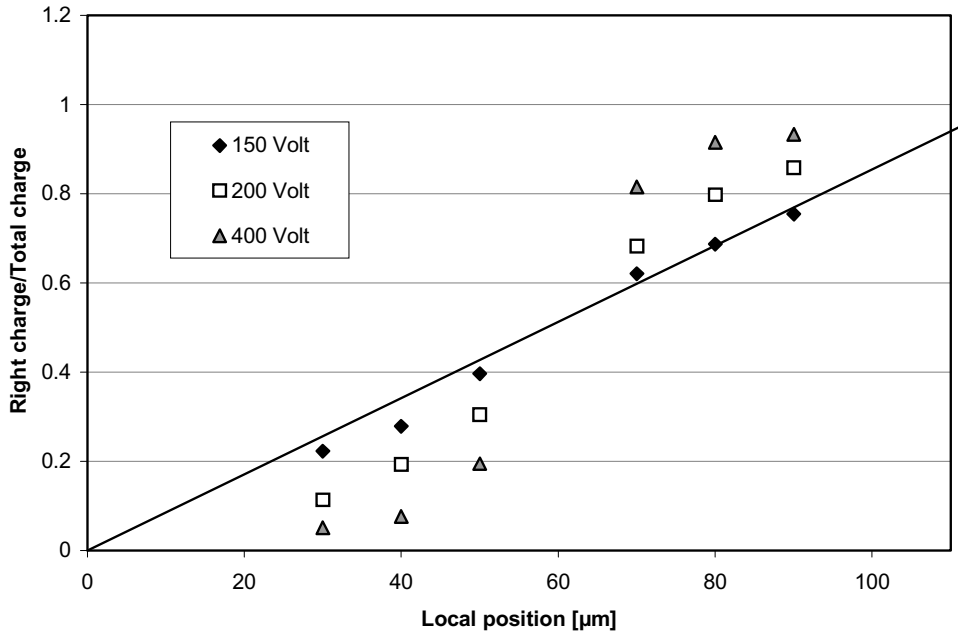

Fig. 10: *η scan across strip #634 – 635 (irradiated region with positive gradient of $|N_{eff}|$ as a function of the strip number). The measuring position was* ***h*** *(see figure 1).*

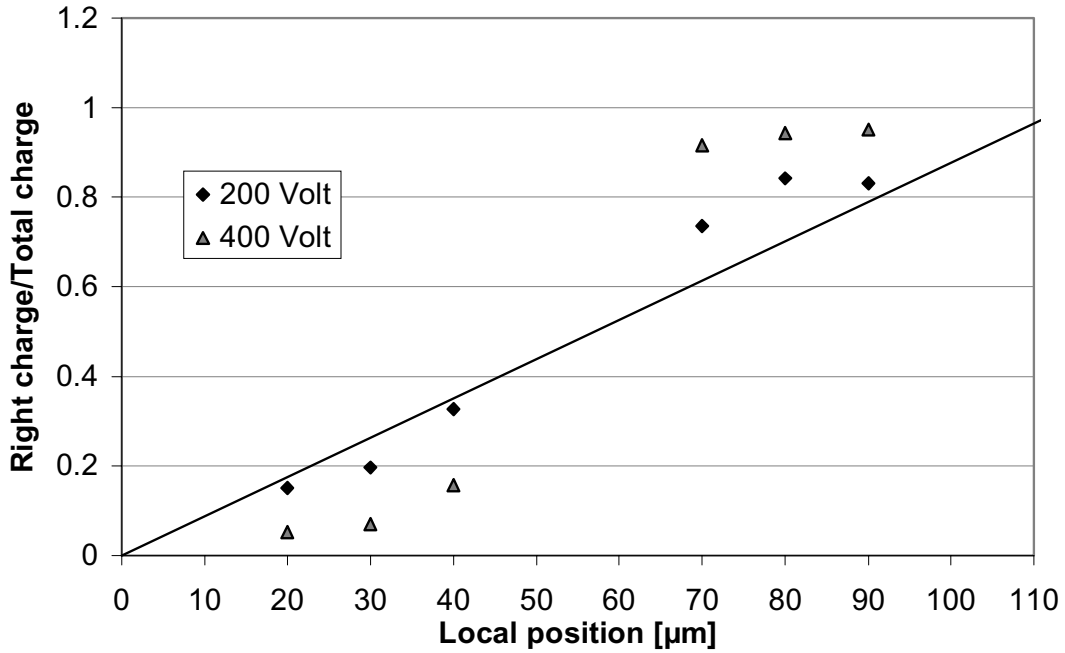

Fig. 11: *η scan across strip #690 – 691 (heavily irradiated region, V_{fd}>200V). The detector was measured at position* ***i****(see figure 1).*

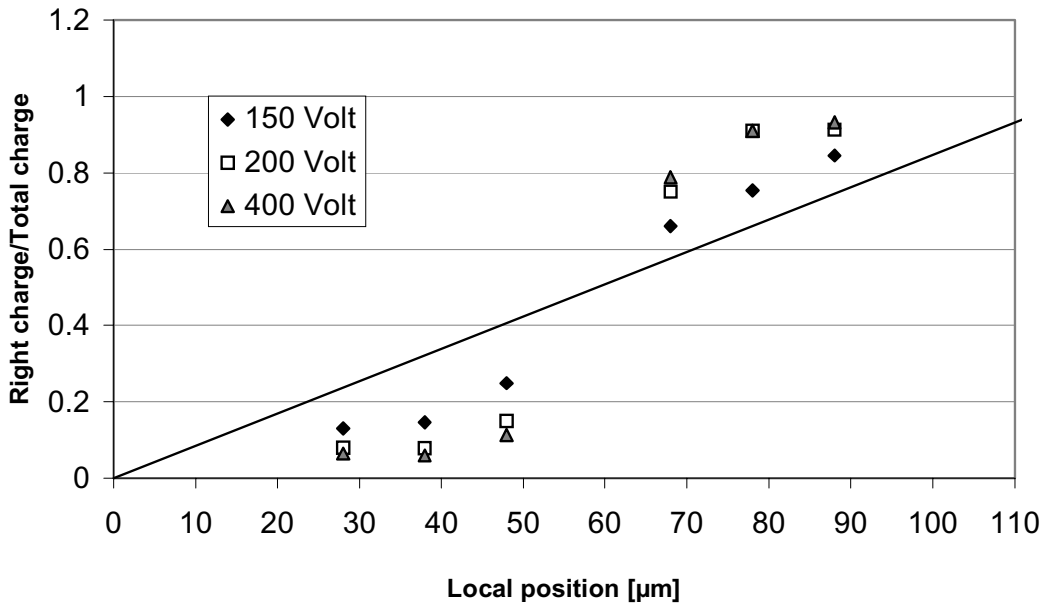

Fig. 12: *η scan across strip #760 - 761 (irradiated region with negative gradient of $|N_{eff}|$ as a function of the strip number). Measured position is at* ***j*** *(see Figure 1).*

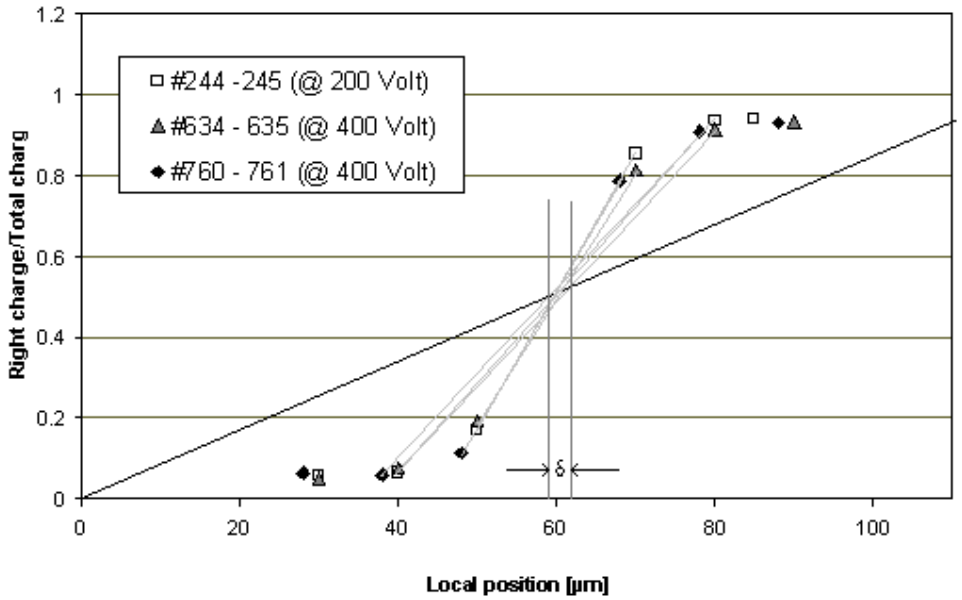

Fig. 13: *Comparison of the η scan across adjacent strips located in the non irradiated, irradiated with positive gradient of V_{fd} and irradiated with negative gradient of $|N_{eff}|$ regions respectively. The degree to which all points from the positive and negative gradient areas on opposite the left and right hands sides of the geometric centre of the strips pass through a common point is a measure of the distortion. The spread observed (δ) is approximately ±2µm. The measured strips #244,634 and 760 correspond to measuring points* ***f,h*** *and* ***e*** *(see Figure 1).*

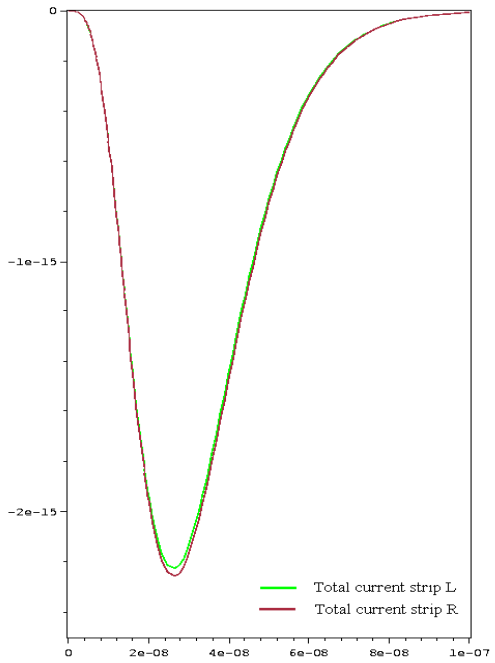

Fig. 14: *ISE simulation of the signal seen by strip L and R in the high gradient ($4.8x10^{12}$ cm^{-4}) region of the N_{eff} profile shown in Fig. 3 for a mip passing in the mid point of the two strips. The signal has been convoluted with the shaping function of a SCT128 chip. The difference between the two signals is about equal to the one seen for a displacement of 1µm towards strip R of the impact point of the mip.*

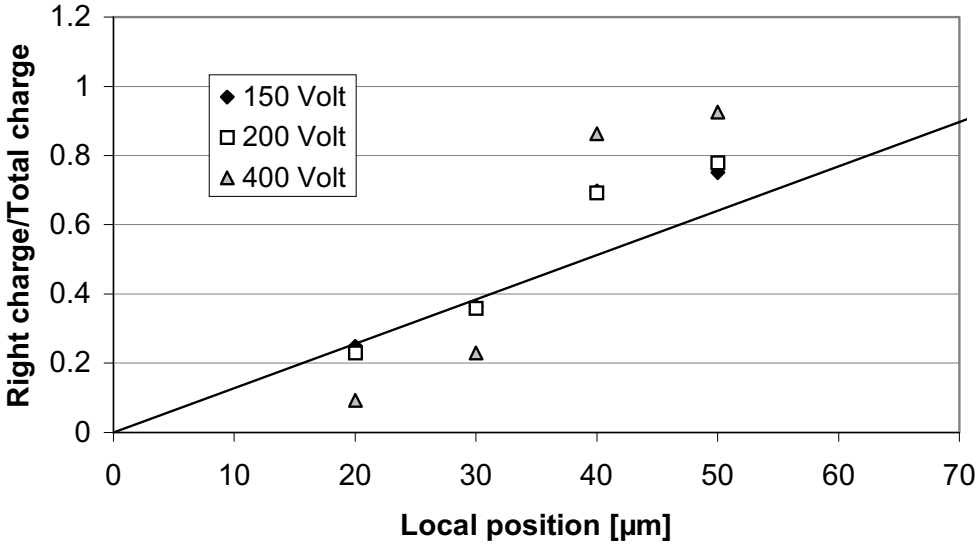

Fig. 15: *η scan across strip #760 – 761 in the inner part (strip pitch 78 µm). Measured position corresponds to* ***i*** *(see Figure 1)*

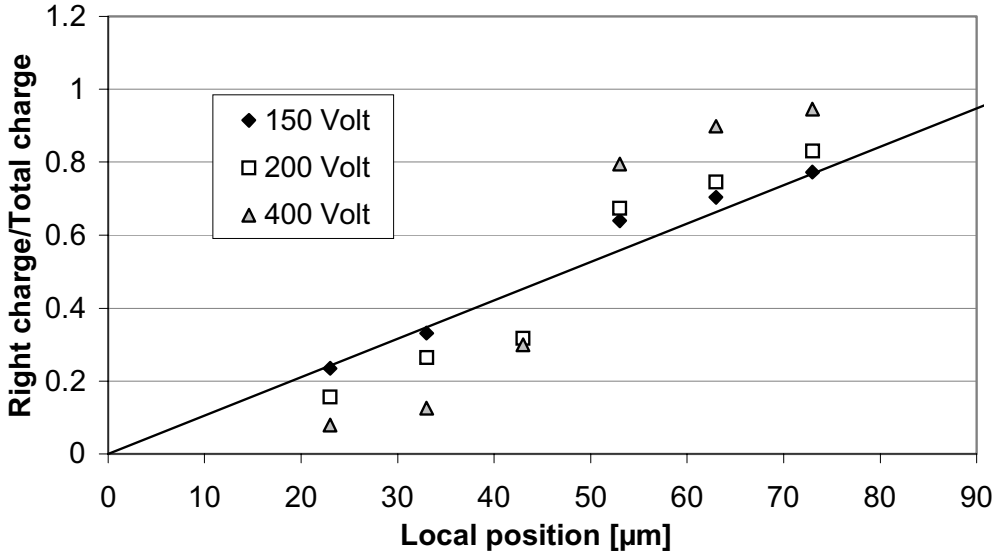

Fig. 16: *η scan across strip #760 – 761 in the intermediate part (strip pitch 95 µm and position* ***j*** *in Figure 1)*

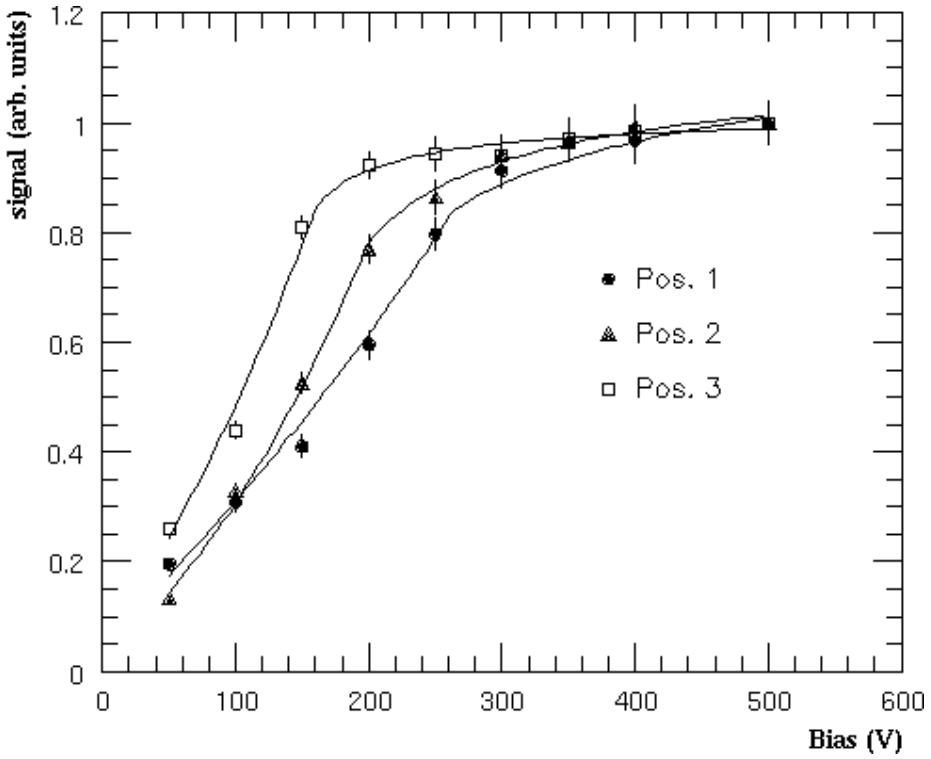

Fig. 17: *CCE curves measured next to strip #760: Pos. 1, 2 and 3 are the inner part, intermediate and outer parts of the strip (measuring points* ***i,j,*** *and* ***e*** *Figure 1).*

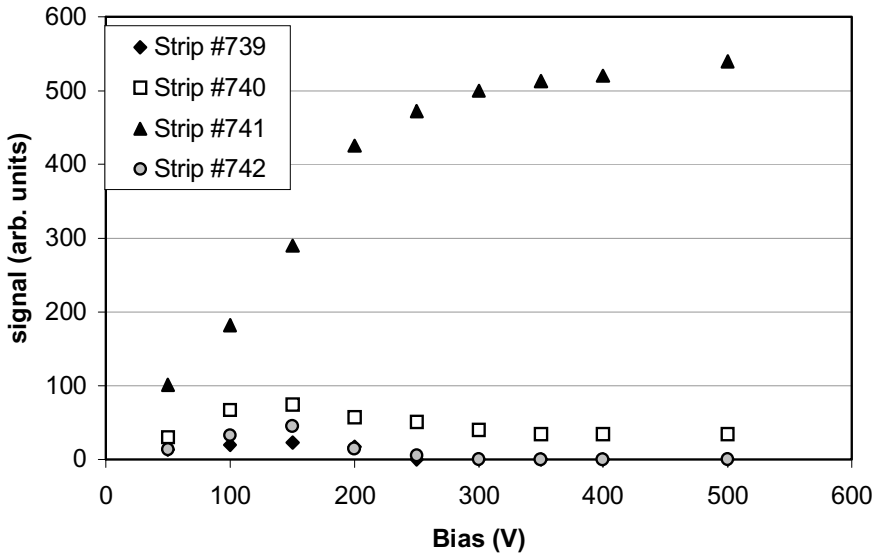

*Fig. 18: Charge collection in four adjacent strips in a irradiated and type inverted region. The laser was focused between strips ~740-741, next to strip #741. (The measuring position was **k**, see Figure 1)*

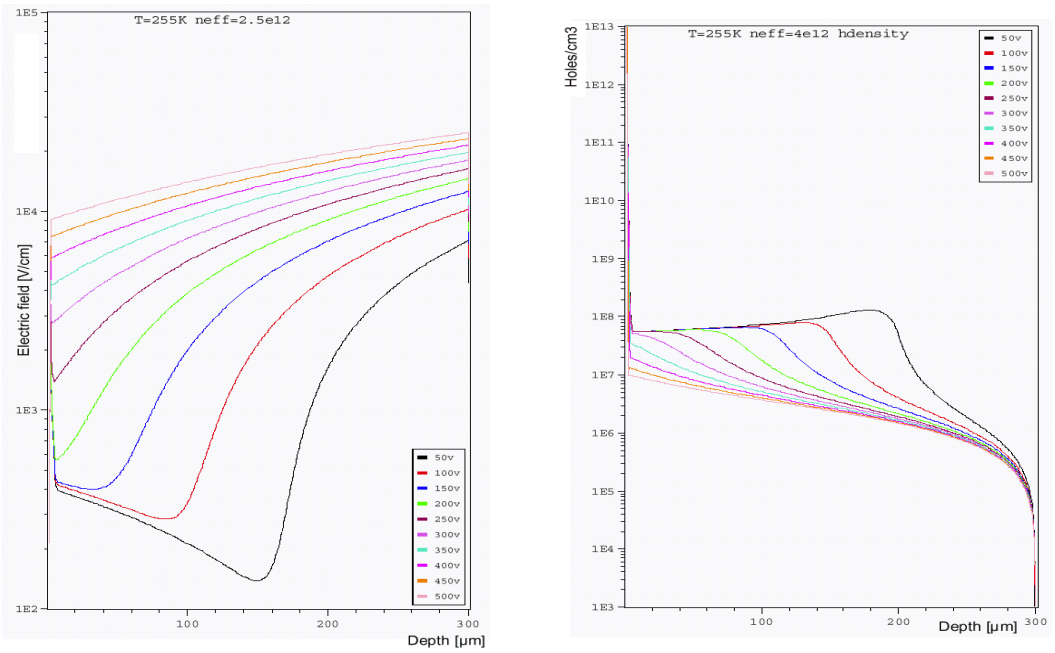

Fig. 19 *Electric field profile and majority carrier concentration in an irradiated ($4x10^{14}$ p cm^{-2}) silicon detector with the bias voltage as a parameter. V_{fd} is ~200V. Note the low density of free charge carrier (right) in the non-depleted bulk (after inversion depletion goes from left to rignt).*

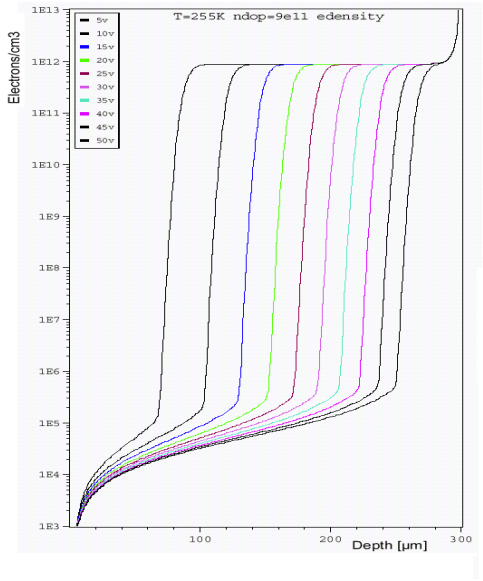

Fig. 20 *Majority carrier concentration in a non irradiated, high resistivity (Neff ~ 10^{12} cm^{-3}) n-type silicon detector with the bias voltage as a parameter. Depletion goes from left to right.*

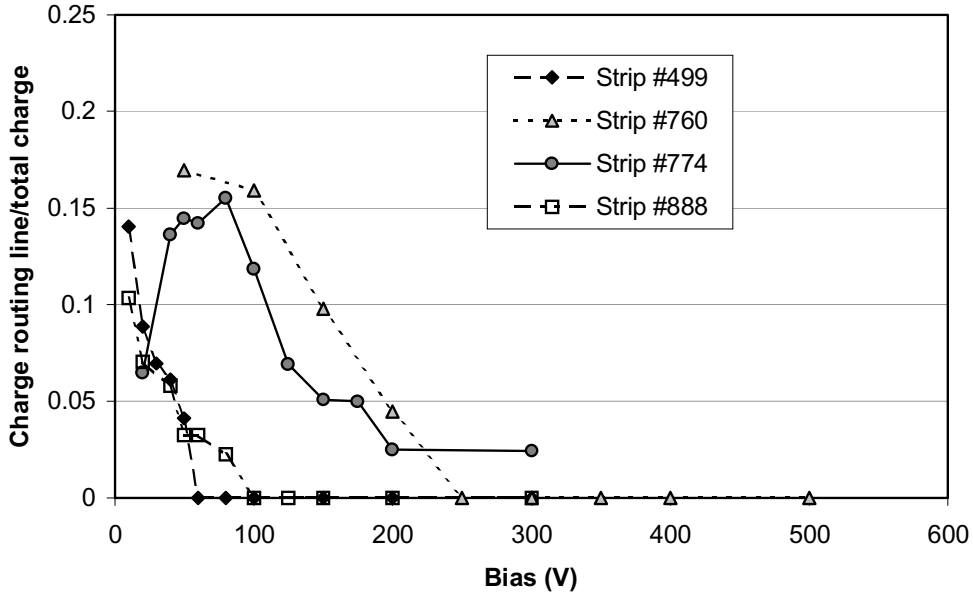

Fig. 21: Ratio between the charge collected by the routing line to the total collected charge in irradiated areas with different fluences. Strips#499,760,774 and 888 were measured at positions ***l,e,m*** *and* ***n*** *(Figure 1).*

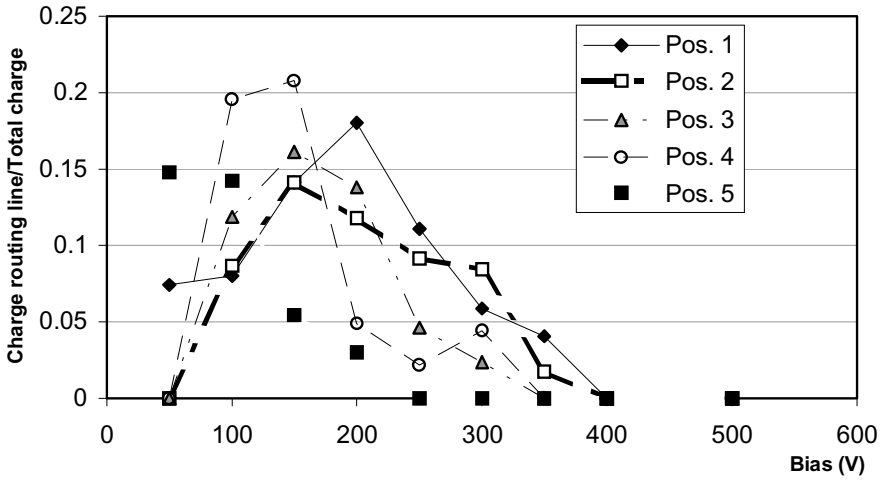

Fig. 22*: Ratio between the charge collected by the routing line to the total collected charge in the proximity of strip #760 in five equally spaced positions from the inner to the outer end of the strip. The shapes of the curves are dependent on the degree of depletion of the sensor at a fixed location and the geometry of the strips (see text). The depletion effects are dominant as there is no trend in maxima from positions 1- 5.*